Korean J. Chem. Eng., **31**(10), 1865-1876 (2014)
DOI: 10.1007/s11814-014-0139-7

pISSN: 0256-1115
eISSN: 1975-7220

Modeling of permeate flux and mass transfer resistances in the reclamation of molasses wastewater by a novel gas-sparged nanofiltration

Tejal Manish Patel and Kaushik Nath†

Department of Chemical Engineering, G H Patel College of Engineering & Technology,
Vallabh Vidyanagar- 388 120, Gujarat, India
(*Received 23 February 2014 • accepted 13 May 2014*)

Abstract−A semi-empirical model has been applied to predict the permeate flux and mass transfer resistances during the cross flow nanofiltration of molasses wastewater in flat-sheet module. The model includes laminar flow regime as well as flow in presence of gas sparging at two different gas velocities. Membrane hydraulic resistance (R_m), osmotic pressure resistance (R_{osm}) and the concentration polarization resistance (R_{cp}) were considered in series. The concentration polarization resistance was correlated to the operating conditions, namely, the feed concentration, the trans-membrane pressure difference and the cross flow velocity for a selected range of experiments. There was an appreciable reduction of concentration polarization resistance R_{cp}^{spar} in presence of gas sparging. Both the concentration polarization resistance R_{cp}^{lam} and osmotic pressure resistance R_{osm} decreased with cross-flow velocity, but increased with feed concentration and the operating pressure. Experimental and theoretical permeate flux values as a function of cross flow velocity for both the cases, in the presence and absence of gas sparging, were also compared.

Keywords: Membrane, Nanofiltration, Flux, Molasses, Gas Sparging, Cross Flow Velocity

INTRODUCTION

Concentration polarization is one of the major bottlenecks of pressure-driven membrane processes towards their widespread commercial acceptance for the reclamation of aqueous waste streams. As filtration proceeds, solute particles accumulate over the septum, forming a polarized layer which grows in thickness. This leads to an increase in osmotic pressure near the membrane-solution interface, thereby decreasing the available driving force (i.e., trans-membrane pressure) and reducing the permeation of solvent. Adhesion forces by which solute particles are attached to the membrane surface are in balance with the shear stress they are exposed to. Therefore, altering the hydrodynamics at the membrane surface towards a more turbulent flow regime proves to be beneficial for their removal [1]. To that end, the use of gas sparging could be a plausible option. Using gas bubbles to enhance membrane processes has been a more recent development. Imasaka et al. first proposed the strategy in 1989 and developed a gas-liquid two-phase cross-flow microfiltration process coupled with an anaerobic digester [2]. The methane generated in the digester, which was injected into ceramic membrane modules, proved to be effective with low energy usage. In a committee report of the American Water Works Association (AWWA) air sparging is mentioned specifically as a method to control fouling by enhancing the shear stress at the membrane surface [3]. Gas sparging in tubular membranes has been established to be a powerful tool for boundary layer and fouling control. Air sparging via the injection of gas bubbles into the feed stream has been applied successfully to the enhancement of ultrafiltration and microfiltration processes involving the separation of many specific compounds or mixtures such as, dextran and bovine serum albumin (BSA) using tubular membrane [4]; hollow fiber membrane [5], yeast suspension in submerged hollow fiber membrane [6], pineapple wine in tubular ceramic membrane [7], dextran T500 in cellulose ester membrane [8], oil-water emulsion [9] and so on. Laborie et al. [10] and Cui et al. [11] give an extensive overview of the literature on air sparging in ultrafiltration. Drews et al. [12] analyzed advantageous and detrimental effects of air sparging in membrane filtration in terms of bubble movement, exerted shear and particle classification. Injecting gas to create a gas-liquid two-phase cross flow ultrafiltration operation can significantly increase permeate flux and, moreover, can improve the membrane rejection characteristics. Controlled pulse injection to generate slug flow becomes more advantageous than uncontrolled gas sparging, especially when the gas flow rate is low [13]. Fulton et al. [14] focused on mapping the shear forces induced by gas sparging in full-scale submerged hollow fiber membrane modules. The shear forces were observed to be highly variable over time and heterogeneously distributed within the system, ranging from 0.1 to over 10 Pa. Chan et al. [15] investigated the bubble-induced shear profiles in submerged hollow fiber membrane modules using an electrochemical method for measuring shear forces [15].

In this paper, our attempt was to study the effectiveness of gas sparging in mitigating the flux decline during cross-flow nanofiltration of molasses wastewater. India has about 200 distilleries spread all over the country and most of those use cane-molasses, a byproduct of cane-sugar plants, as the raw materials. In almost all the distilleries, batch fermentation mode is adopted whereby 12-15 liters of spent wash is generated per liter of alcohol production. Molasses-based distilleries are one of the most polluting industries in India, generating large volumes of high strength wastewater with high concentration of organic matters, and several nutrients in the form of ni-

†To whom correspondence should be addressed.
E-mail: kaushiknath2003@yahoo.co.in

trogen, phosphorus and potassium, leading to eutrophication of water bodies [16]. Further, its dark color due to the presence of melanoidin pigment hinders photosynthesis by blocking sunlight and is therefore deleterious to aquatic life. Adequate treatment is thus crucial before the effluent is discharged. In a recent study Nataraj et al. [17] reported pilot trials on distillery spent wash using a hybrid nanofiltration (NF) and reverse osmosis (RO) process with thin film composite (TFC) membranes in spiral wound configuration. NF was primarily effective in removing the color and colloidal particles accompanied by 80%, 95% and 45% reduction in total dissolved solids (TDS), conductivity and chloride concentration, respectively, at an optimum feed pressure of 30-50 bar. The subsequent RO operation at a feed pressure of 50 bar resulted in 99% reduction each in COD, potassium and residual TDS. Rai et al. [18] carried out tertiary treatment of distillery wastewater by nanofiltration in a spiral wound module. The color and chemical oxygen demand (COD) removal were in the range of 98-99.5%. Another study [19] reports the separation of saccharides from a NaCl solution by using polyamide/polysulfone nanofiltration membranes.

The use of gas sparging in nanofiltration of molasses waste water may be an effective method to improve the permeate flux. Although a few types of feeds have been used to investigate the effect of gas sparging on the permeate flux, no results are reported so far using molasses waste water as the feed.

This study is therefore not a classical nanofiltration study considering the rejection of pollutants from wastewater, but a novel approach in which gas sparging provides gas-liquid flow conditions promoting sustainable volumetric flux. Additionally, it is important to understand the performance of a gas-sparged NF system, especially the rejection of solutes and the permeate flux, under certain operating conditions in order to optimize the application and operation of the NF membrane. In light of the above, our objective was to develop a semi-empirical, resistance in series model to predict the permeate flux and mass transfer resistances based on simultaneous solution of film theory and solution-diffusion model. The modeling was applied to both the cases, with and without gas sparging. It was based on the assumption that the hydraulic and the osmotic pressure resistance and a concentration polarization resistance, which was a function of the operating conditions, acted in series to take into account the flux decline under steady state condition. The correlation for the concentration polarization resistance with the operating conditions was developed using some selected experimental data, and the osmotic pressure controlled flux was therefore predicted using the correlation.

MODELING THEORY

1. Solution Diffusion Model

The transport equation through the porous membrane can be given by the following solution-diffusion model to describe the osmotic pressure controlled flux:

$$v_w^{osm}=L_p(\Delta P-\Delta\pi) \tag{1}$$

where, $L_p=(1/\mu R_m)$ indicates the permeability of the membrane. This permeability is related to the traditional Darcy's permeability (k_o) as, $L_p=k_o/\mu\delta$, where, δ is the thickness of the membrane skin and μ is the viscosity of the permeating solution.

The osmotic pressure difference across the membrane is given by

$$\Delta\pi=\pi_m-\pi_p \tag{2}$$

where, π_m is the osmotic pressure at the membrane surface and π_p is that in the permeate stream. Since osmotic pressure is a colligative property, it is expressed as a linear function of solute concentration according to van't Hoff's law (valid for dilute solutions, as is the case for the experiments reported herein)

$$\pi=ac$$

where, the osmotic coefficient a is given as

$$a=\frac{RT}{M} \tag{3}$$

Using room temperature and molecular weight of molasses (average molecular weight: 1165 as determined by the gel permeation chromatography; universal gas constant R: 8,314 J $mol^{-1}K$; T: 303 K), the osmotic pressure becomes

$$\pi=2162c \tag{4}$$

The membrane-solute system is characterized by parameter real retention, R_r, which is constant for a particular membrane-solute combination. The real retention, which is a constant for a membrane-solute system, is defined as

$$R_r=1-\frac{c_p}{c_m} \tag{5}$$

Using Eqs. (1)-(5), the osmotic pressure controlled flux is expressed as

$$v_w^{osm}=L_p(\Delta P-2062c_mR_r) \tag{6}$$

The osmotic pressure controlled flux, v_w^{osm} cannot be calculated from Eq. (6), as c_m is unknown. For that, the film theory for steady state mass transfer is used, as discussed in the following section.

2. Film Theory Model

When solutes are rejected in a steady-state NF membrane separation process, the local solute concentration at the membrane surface (c_m) reaches its maximum and the solute flux is constant through the membrane and equals the solute flux through the membrane, v_w^{osm}. Based on the above film theory, the material balance for the solute in a differential form can be presented. A constant film of solutes is assumed to develop on the surface of the membrane.

Fig. 1 presents the schematic representation of solute transport. At steady state, the net solute flux towards the membrane is zero and the solute balance equation in the stagnant film of the solutes near the membrane surface results in

$$v_w^{osm}c+D\frac{dc}{dy}=v_w^{osm}c_p \tag{7}$$

On integrating Eq. (7) from y=0, $c=c_m$ to $y=\delta$, $c=c_0$, the standard film theory equation is obtained as represented by

$$v_w^{osm}=k\ln\left[\frac{c_m-c_p}{c_o-c_p}\right] \tag{8}$$

The permeate concentration c_p can be expressed in terms of the mem-

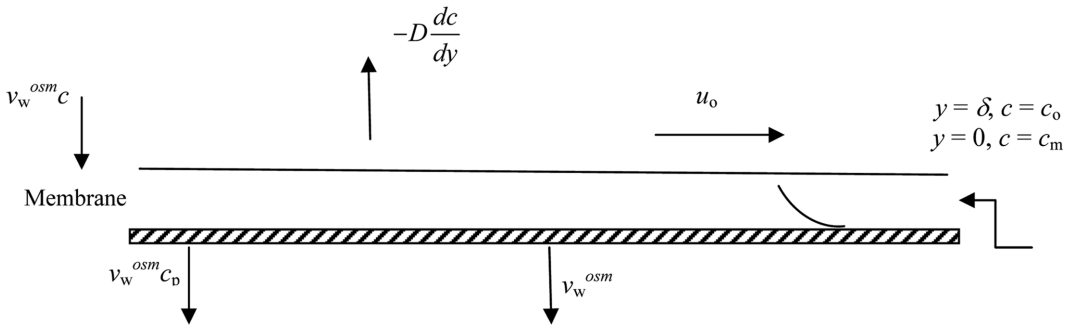

Fig. 1. Schematic representation of boundary layer transport model for flow through membrane under applied transmembrane pressure.

brane surface concentration, c_m and R_r from Eq. (5).

Eq. (8) can be expressed as

$$v_w^{osm} = k\ln\left(\frac{c_m R_r}{c_0 - c_m(1-R_r)}\right) \tag{9}$$

For the same solute and system geometry, an increase in Re increases forced convection and, consequently, the growth of the concentration boundary-layer is minimized so that the Sherwood number increases. Now, for the description of a realistic mass transfer operation in a conduit it is convenient to work with an average mass transfer coefficient and an average Sherwood number relationship. In general, the Sherwood (Sh) number is related to the Schmidt (Sc) and Reynolds (Re) numbers for laminar flow as follows:

$$Sh = \frac{kd_e}{D} = 1.85\left(ReSc\frac{d_e}{L}\right)^{1/3} \tag{10}$$

The Graetz-Leveque's correlation (Eq. (10)) is valid for flow in impervious conduits [20] and it is mostly used in today's membrane literature. However, the effect of wall porosity (or suction) is important only in the cases of relatively open membranes, e.g., UF and MF membranes as was shown by De and Bhattacharya [21] and Minnikati et al. [22]. Therefore, the equation in its present form can safely be used in the nanofiltration for the present system.

For turbulent flow conditions (Re>2000-4000) Harriott-Hamilton correlation was used to calculate Sh [23].

$$Sh = 0.0096Re^{0.91}Sc^{0.35} \tag{11}$$

For the determination of diffusivity D, the correlation of Wilke and Chang [24] was used.

$$D = \frac{(117.3\times10^{-18})(\phi M)^{0.5}T}{\mu v^{0.6}} \tag{12}$$

where M is the molecular weight of the solvent, μ solution viscosity, v solute molar volume and φ association factor for solvent.

Equating Eqs. (6) and (9), the following equation is obtained:

$$v_w^{osm} = L_p(\Delta P - 2062 c_m R_r) = k\ln\left(\frac{c_m R_r}{c_0 - c_m(1-R_r)}\right) \tag{13}$$

Eq. (13) can be solved by trial and error using a suitable method, e.g., Newton-Raphson algorithm, to determine c_m and hence v_w^{osm}. Once c_m calculated from Eq. (13) the permeate concentration c_p can be estimated from Eq. (5).

The osmotic pressure resistance, R_{osm} is calculated as follows:

$$v_w^{osm} = \frac{\Delta p}{\mu(R_m + R_{osm})} \tag{14}$$

or

$$R_{osm} = \left(\frac{\Delta P}{\mu v_w^{osm}} - R_m\right) \tag{15}$$

The actual experimental flux is observed to be much lower than the osmotic pressure controlled flux due to the formation of the concentration polarization layer. Therefore, the final experimental flux can be written in terms of the concentration polarization resistance as

$$v_w^{expt} = \frac{\Delta P}{\mu(R_m + R_{osm} + R_{cp}^{lam})}$$

or

$$v_w^{expt} = \frac{(\Delta P - \Delta\pi)}{\mu(R_m + R_{cp}^{lam})} \tag{16}$$

Eq. (16) can be further simplified as,

$$v_w^{expt} = \frac{(\Delta P - \Delta\pi)}{\mu R_m(1 + R_{cp}^{lam}/R_m)} = \frac{v_w^{osm}}{(1 + R_{cp}^{lam}/R_m)} \tag{17}$$

Having calculated v_w^{osm} from Eq. (9), R_{cp}^{lam} can be obtained from Eq. (17) using the experimental flux values. The gel type layer r resistance is actually determined by the membrane surface concentration (c_m) and its thickness. Both c_m and the thickness of the gel-type layer cannot be measured easily. However, c_m can be expressed as a function of the operating variables: pressure, initial concentration and the cross flow velocity. Therefore, the resistance is expressed in terms of these variables.

$$R_{cp}^{lam} = \alpha(\Delta P)^{n_1}(u_o)^{n_2}(c_o)^{n_3} \tag{18}$$

Sparging of gas is thought to promote turbulence. Hence, the resistance offered to the solvent flux by the concentration polarization layer should be less while gas sparging is on. This is supported by the experimental findings of appreciably less decline in permeate flux in presence of gas sparging at two different gas velocities. It is to be emphasized that the effect of this localized turbulence does not change the membrane surface concentration as compared to the case of no gas sparging for the same operating conditions. It has been experimentally observed that the concentrations of the permeate streams remain unaffected with respect to the presence or absence of the gas sparging for the same set of operating condi-

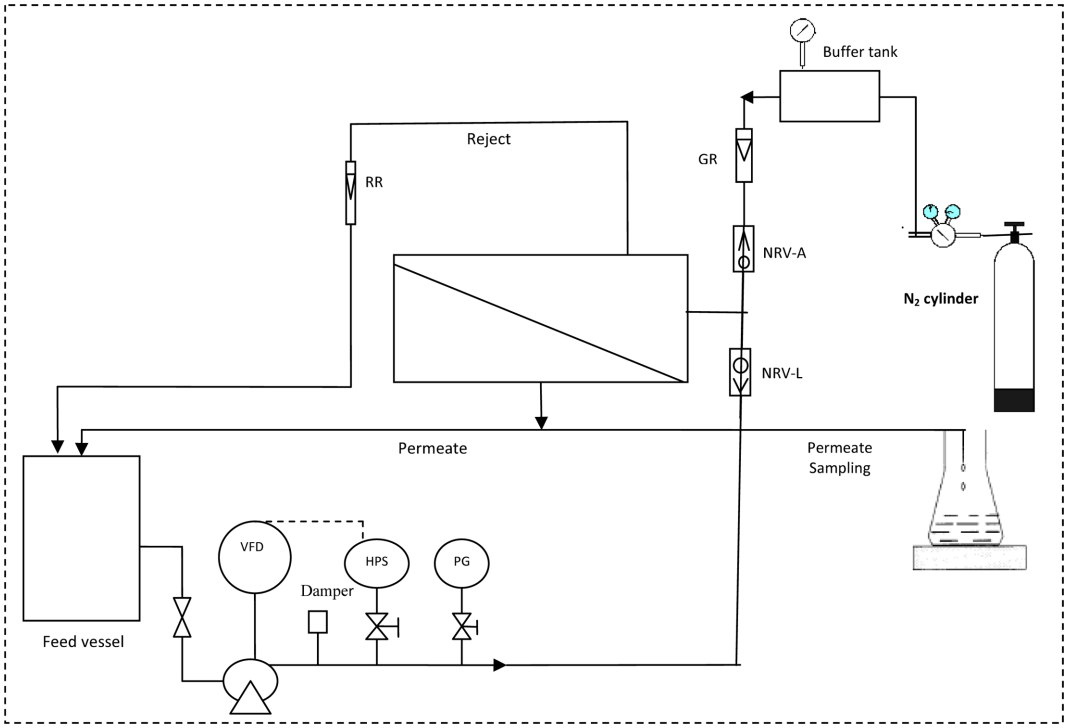

Fig. 2. Schematic of experimental set-up of gas-sparged nanofiltration (VFD: variable frequency device; HPS: high pressure switch; PG: pressure gauge; RR: reject rotameter, GR: gas rotameter; NRV-A: non return valve for air; NRV-L: non return valve for liquid).

tions. Since R_r is constant for a particular membrane-solute system, it may be observed from Eq. (5) that the membrane surface concentration, c_m should remain the same, even in the case of the experiments with gas sparging. Therefore, as long as the feed velocity (and the other operating conditions) is constant, c_m remains unaffected. Therefore, the external mass transfer is still governed by Eq. (10) as in the laminar flow case without gas sparging. This indicates that the osmotic pressure controlled flux, v_w^{osm} remains unchanged, as observed by some other researchers [26]. Using experimental flux values, the concentration polarization resistance for various operating conditions with gas sparging is calculated and correlated with the operating condition as

$$R_{cp}^{spar} = \beta(\Delta P)^{m_1}(u_o)^{m_2}(c_o)^{m_3} \quad (19)$$

MATERIALS AND METHODS

1. Chemicals

Molasses, obtained from Shree Vadodara District Cooperative Sugarcane Factory, Baroda, India, was stored at 5-6 °C in the refrigerator and was used on as-received basis. However, it was diluted with distilled water, and three different concentrations, namely 1 kg m^{-3}, 2 kg m^{-3} and 4 kg m^{-3}, were used in the present study. The pH was 5.2±0.2, water content 15-20%, ash content 15%, and density 1.292 g/L. All other chemicals used in this experiment were of AR grade supplied by Merck, India and were used without further purification.

2. Membranes

Hydrophilized polyamide (PA-NF) membrane of thickness 125 micron and MWCA (molecular weight cut off) 250, with support cloth was used in the study. The membrane was supplied by M/s Permionics Membrane Pvt. Ltd., Baroda, India. It is a thin-film composite membrane element consisting of a non-woven polyester substrate on which a polyethersulfone layer is coated. The membrane was prepared by solution casting and phase inversion gelling. The effective membrane area was 0.016 m^2.

3. Experimental Set-up

The experimental set-up, is schematically illustrated in Fig. 2, consisted of a cross flow nanofiltration unit with a flat sheet membrane housed in a stainless steel test cell. Feed solution from the feed tank was pressurized by high pressure plunger pump (50-400 psi) and entered in to the test cell. Nitrogen gas from a cylinder was introduced to the inlet of the flat sheet module, via the buffer tank (to reduce the pressure fluctuation of the incoming gas) through a T-piece connector having ID of 4 mm. The gas was injected with the feed in co-current flow manner. The gas flow rate was controlled by means of a gas rotameter. Two non-return valves (NRV) were provided, one at the gas inlet and the other at the feed inlet line in order to prevent the back flow of air or liquid as the case may be. Experiments were carried out in the total recycle mode of filtration (TRMF). Reject stream was collected and recycled to the feed tank routed through a rotameter. The permeate stream was also recycled to maintain a constant concentration in the feed tank since the feed volume was kept constant throughout the experiment. The permeate samples were collected and analyzed for various parameters such as TDS, conductivity, COD. Nanofiltration was carried out for 1 h duration with the cumulative filtrate volume monitored throughout the experiment.

4. Permeate and Reject Concentration

Color intensity of the permeate and reject streams was measured by a HACH DR-2010 model spectrophotometer following USEPA

approved HACH method # 8000 [27]. For color measurements, this device was calibrated at a wavelength of 455 nm with Pt-Co standard solution. Concentrations of salts (single salt solutions only) were determined by conductivity, measured at 25±0.5 °C using an auto-ranging conductivity/TDS meter (Hanna Instruments, Taiwan).

5. Measurement of COD, TDS, pH and Conductivity

Chemical oxygen demand (COD), total dissolved solid (TDS), pH and conductivity of the feed and permeate streams were measured following standard methodologies [27].

6. Estimation of Model Parameters

The membrane permeability Lp was measured by experiments using pure distilled water. Water fluxes at various pressures were measured and the membrane permeability was calculated from the slope of the permeate flux versus pressure plot. The hydraulic resistance of the membrane was calculated from the definition

$$R_m = \frac{1}{\mu L_p} \tag{20}$$

The osmotic pressure (π) with concentration was calculated using van't Hoff's equation (Eq. (4)).

7. Correlation for the Concentration Polarization Resistance (R_{cp}^{lam} and R_{cp}^{spar})

The concentration polarization resistances in absence of gas sparging and with gas sparging were calculated and were fitted in Eq. (18) and Eq. (19), respectively. The values of the parameters were obtained by multiple log-linear regression method.

8. Determination of Shear Stress Number

It is known that an increase in cross flow velocity and/or gas injection leads to an increase in wall shear stress on the membrane surface. A dimensionless shear stress number (N_s) was introduced to compare the shear stress at the membrane wall and the driving force (trans-membrane pressure) [28]. In the absence of gas sparging (single-phase flow), the dimensionless shear stress number is:

$$N_s = \frac{\rho_{liq} u_{liq}^2}{TMP} \tag{21}$$

If gas sparging is applied (two-phase flow), the generalized shear stress number is

$$N_s' = \frac{\rho_{mixture} u_{mixture}^2}{TMP} \tag{22}$$

where ρ_{liquid} and $\rho_{mixture}$ are the liquid density and mixture density (kg m^{-3}), respectively, u_{liquid} and $u_{mixture}$ are the superficial liquid velocity and mixture velocity (ms^{-1}), respectively, and TMP is the trans-membrane pressure (Pa). The TMP at specified condition (for example at critical flux or at limiting flux) is used to calculate the corresponding shear stress number.

The mixture velocity can be taken as:

$$u_{mixture} = u_{liq} + u_{gas} \tag{23}$$

The mixture density can be calculated as follows:

$$\rho_{mixture} = \frac{\rho_{gas} u_{gas} + \rho_{liq} u_{liq}}{u_{mixture}} \tag{24}$$

9. AFM and SEM Microscopy

Atomic force microscopy (AFM) was carried out using a NT-MDT NTEGRA Aura Autoprobe CP atomic force microscope. Measurements were performed on the dry membrane samples under ambient atmospheric conditions. Silicon cantilevers with integrated pyramidal tips were used to image membrane surface topography. The membrane surfaces were imaged in tapping mode. Differences in the membrane surface morphology can be expressed in terms of various roughness parameters such as the average roughness and the root means square (RMS) roughness. The average roughness is defined as the average deviation of peaks and valleys from the mean plane, and the RMS roughness is the deviation of peaks and valleys from the mean plane. At least three separate scans, each covering an area of 100 μm^2, were acquired on each membrane to determine the mean roughness values. The surface roughness was reported in terms of the root mean square roughness (RMS) and calculated by using Eq. (25),

$$RMS = \sqrt{\frac{\sum (Z_{cu} - Z_{av})^2}{p}} \tag{25}$$

where Z_{av} is the average of the z values within the given area; Z_{cu} is the current z value; and p is the number of points within a given area. The surface roughness parameter was calculated from the AFM images using an AFM software program. The SEM analysis of the pristine (unused) and fouled membranes was done on Leo 1430VP (England). All membrane samples were dried overnight at 40 °C before preparing 3 mm×3 mm strips for silver sputter coating. The silver-coated strips were used for recording the SEM images.

RESULTS AND DISCUSSION

1. Effect of Gas Sparging on Various Resistances

Experimental permeate concentrations and the magnitudes of various resistances at three different trans-membrane pressures and cross flow velocities are compared in Table 1 for both the cases: in presence and absence of gas sparging. Gas sparging involved using two different gas velocities: 0.4 m/s and 0.8 m/s. Resistance as a result of concentration polarization is the major reversible resistance leading to a decline of flux over time in nanofiltration operation. Concentration polarization resistance (R_{cp}^{lam}) was calculated by using Eq. (18) in absence of gas sparging. Experimental data were selected to encompass the entire experimental range (in terms of pressure, feed concentration and cross flow velocity). The values of the parameters were obtained by multiple log-linear regression method and were estimated to be ln α=27.99, n_1=0.25, n_2=−0.15, n_3=0.81. The correlation coefficient of this fit was 0.98. It may be observed that the exponents n_1 and n_3 (associated with ΔP and c_o, respectively) are positive and n_2 (associated with cross flow velocity) is negative. This clearly indicates that the concentration polarization resistance at steady state increased with the operating pressure and feed concentration as these conditions favored high polarization. On the other hand, concentration polarization resistance decreased with cross flow velocity, due to increased forced convection of the solute particles. Concentration polarization resistance in presence of gas sparging (R_{cp}^{spar}) was calculated by using Eq. (19) incorporating gas sparging conditions at both the gas velocities 0.4 m/s and 0.8 m/s and for feed concentrations of 4,000 mg/L and 2,000 mg/L. For the experiments in presence of gas sparging, the selected experiments for the development of the concentration polarization resistance are shown in

Table 1. Permeate concentration, mass transfer coefficients and resistances in presence and absence of gas sparging in the nanofiltration of molasses wastewater

Sl. No	TMP (kPa)	u_l (m/s)	N_{Re}	c_p (kg/m^3)	$k\times10^{-4}$ m/s	$R_{osm}\times10^{13}$ (m)	$R_{cp}\times10^{13}$ (m)
No gas sparging ($R_{cp}=R_{cp}^{lam}$)							
1	490	0.2	941.2	0.075	0.0893	33.1	17.22
2		0.35	1647	0.0675	0.107	29.7	16.76
3		0.45	2017.2	0.0536	0.194	23.5	16.15
4	686	0.2	941.2	0.0964	0.0893	33.4	17.94
5		0.35	1647	0.0833	0.107	19.1	17.05
6		0.45	2017.2	0.0603	0.194	18.8	16.82
7	980	0.2	941.2	0.1398	0.0893	33.8	22.35
8		0.35	1647	0.1139	0.107	25	18.48
9		0.45	2017.2	0.072	0.194	22.6	17.31
Gas sparging at u_g=0.4 m/s; ($R_{cp}=R_{cp}^{spar}$)							
10	490	0.2	2715.1	0.0504	0.2466	19.04	12.56
11		0.35	3450.6	0.0482	0.3049	11.14	11.77
12		0.45	3930.2	0.0472	0.3417	8.75	11.29
13	686	0.2	2715.1	0.0553	0.2466	18.9	14.86
14		0.35	3450.6	0.052	0.3049	11.04	13.95
15		0.45	3930.2	0.0505	0.3417	8.66	13.62
16	980	0.2	2715.1	0.0636	0.2466	18.81	14.84
17		0.35	3450.6	0.0583	0.3049	10.97	14.21
18		0.45	3930.2	0.0559	0.3417	8.59	13.93
Gas sparging at u_g=0.8 m/s; ($R_{cp}=R_{cp}^{spar}$)							
19	490	0.2	4358.6	0.0464	0.3844	36.32	12.63
20		0.35	5175.7	0.0455	0.4444	21.54	11.79
21		0.45	5680.7	0.045	0.4821	16.96	10.86
22	686	0.2	4358.6	0.0493	0.3844	36.09	12.85
23		0.35	5175.7	0.0479	0.4444	21.38	12.38
24		0.45	5680.7	0.0472	0.4821	16.83	11.87
25	980	0.2	4358.6	0.0539	0.3844	35.92	11.07
26		0.35	5175.7	0.0518	0.4444	21.27	10.76
27		0.45	5680.7	0.0508	0.4821	16.72	10.54

Table 1. The values of the exponents were ln β=26.37, m_1=0.38, m_2=−0.089, m_3=0.71. Note that the overall impact of the Eq. (18) and (19) is in line with the expected trend, i.e., R_{cp} in presence of gas sparging was less than that without sparging.

Table 1 indicates that there is an appreciable reduction of concentration polarization resistance R_{cp}^{spar} in presence of gas sparging. Both the concentration polarization resistance R_{cp}^{lam} and osmotic pressure resistance R_{osm} decrease with cross-flow velocity, increase with feed concentration and the operating pressure. This trend is quite expected as higher feed concentration and lower cross-flow velocity favor concentration polarization. Membrane hydraulic resistance (R_m) was found to be 4.5×10^{13} m^{-1}, which remained constant under all experimental conditions. For example, under 'no gas sparging condition' R_{cp}^{lam} at the same cross flow velocity of 0.35 ms^{-1} increased from 17.05×10^{13} m to 18.48×10^{13} m with increase in transmembrane pressure from 686 kPa to 980 kPa. But it decreased from 22.35×10^{13} m to 17.31×10^{13} m with increase in cross flow velocity (CFV) from 0.2 to 0.45 ms^{-1} at a fixed pressure of 980 kPa and feed concentration of 4 kg m^{-3}. In case of R_{osm}, the value decreased from 33.8×10^{13} m to 22.6×10^{13} m with increase in velocity, and it increased from 19.1×10^{13} m to 25×10^{13} m with increase in pressure (from 686 kPa to 980 kPa). It indicates that with increase in CFV of liquid permeate flux increases, as increase of the tangential liquid velocity usually leads to a decrease in concentration polarization and consequently to a decreased resistance [16]. The same trend of reduction of R_{cp} with increasing cross-flow velocity was also observed when gas sparging was initiated using two different gas velocities, although the magnitude of concentration polarization resistance under gas-sparged conditions R_{cp}^{spar} was considerably less compared to the condition of 'no gas sparging'. At the TMP of 980 kPa the values of R_{cp} were 22.35×10^{13} m and 18.48×10^{13} m at CFVs of 0.2 and 0.35 ms^{-1}, respectively, when there was no gas sparging. But at the same TMP with gas sparging at velocity (u_g) of 0.4 m/s the values of R_{cp} were found to be 14.84×10^{13} m and 14.21×10^{13} m at CFVs of 0.2 and 0.35 ms^{-1}, respectively. This was corresponding to almost 33.6% and 23% reduction of concentration polarization resistance under the influence of gas sparging at CFVs of 0.2 and 0.35 ms^{-1}, respectively. The basic mechanism of the enhancement by gas sparging

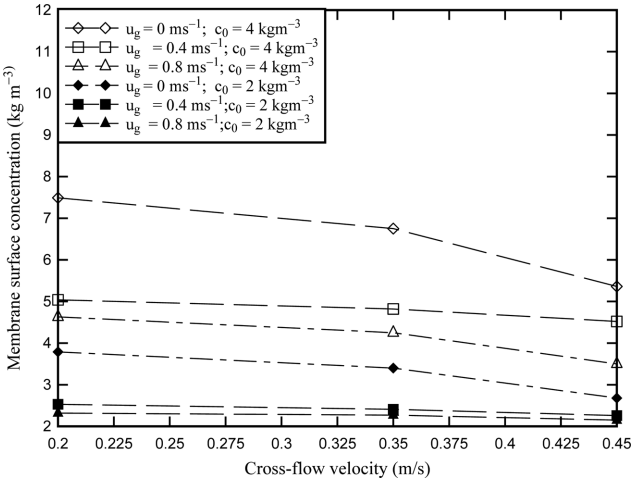

Fig. 3. Variation of membrane surface concentration with cross-flow velocity at constant transmembrane pressure of 680 kPa.

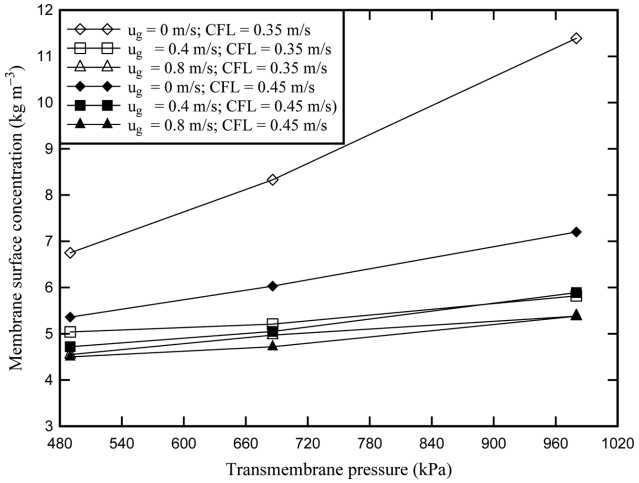

Fig. 4. Variation of membrane surface concentration with transmembrane pressure under different conditions of gas sparging and cross-flow velocity.

in the membrane filtration can be ascribed to the secondary flow induced by air bubbles, which facilitates local mixing, thereby reducing the thickness of mass transfer boundary layer. As a result, the rate of mass transfer of solute molecules from the membrane surface back to the bulk solution is increased and the wall concentration is reduced [29]. However, the experimental results found in this study are not in agreement with those reported by Ducom and Cabassud [28], who did not find any beneficial effects of air sparging, due to high shear liquid flow in the system and the maldistribution of bubbles in the flat sheet module [30].

2. Membrane Surface Concentration

The membrane surface concentration c_m was calculated by the Newton-Raphson method after finding the root of the equation formed by the difference between v_w^{osm} (Eq. (6)) and v_w^{osm} (Eq. (8)) for operating conditions expressed as Eqs. (6), (8) and (9). The variation of c_m with the cross flow velocity (CFL) at two different feed concentrations but at constant transmembrane pressure of 680 kPa is presented in Fig. 3. From Fig. 3, the membrane surface concentration decreased with the cross flow velocity due to the forced convection. A similar trend was observed for both in presence and absence of gas sparging. Moreover, at a constant feed concentration and transmembrane pressure the decrease in the membrane surface concentration with cross flow velocity was more pronounced in presence of gas sparging. Thus, according to the model calculation, at TMP of 686 kPa and CFL 0.35 m/s, for c_o 4 kg m^{-3}, the value of c_m was 8.33 kg m^{-3} in absence of gas sparging. But the values of c_m were reduced to 5.21 kg m^{-3} and 4.97 kg m^{-3} with gas sparging at gas velocities of 0.4 ms^{-1} and 0.8 ms^{-1}, respectively. Again at CFL of 0.45 m/s, for the same TMP and initial feed concentration, the values of c_m were 6.03, 5.05 and 4.72 kg m^{-3} for the conditions of 'no sparging', 'sparging with 0.4 ms^{-1} gas velocity' and 'sparging with 0.8 ms^{-1} gas velocity', respectively. The same descending trend of membrane surface concentration with gas sparging was also observed for other operating conditions as well.

Fig. 4 shows the membrane surface concentration (c_m) in the cross-flow NF cell with transmembrane pressure at different cross-flow velocities for 2 kg m^{-3} and 4 kg m^{-3} feed concentrations (c_o). Concentration polarization increased with feed concentration. The value of c_m was higher than that of c_0 under all the operating conditions. With an increase in the cross-flow velocity, c_m is reduced as solute particles were swept away from the surface of the membrane by forced convection imposed by cross flow of the feed solution. As pressure increases, the solute flux towards the membrane is more due to convection, leading to an increase in the membrane surface concentration. With increase in feed concentration the osmotic pressure of the solution at the membrane surface increases, leading to a reduction in the driving force for the solvent flux through the membrane. As a result, water flux decreases and membrane surface concentration increases. Similar observation was reported by Auddy et al. [25] during the turbulent promoter enhanced nanofiltration of dye solutions.

3. Shear Stress Number

The values of shear stress number (N_s) at three different cross-

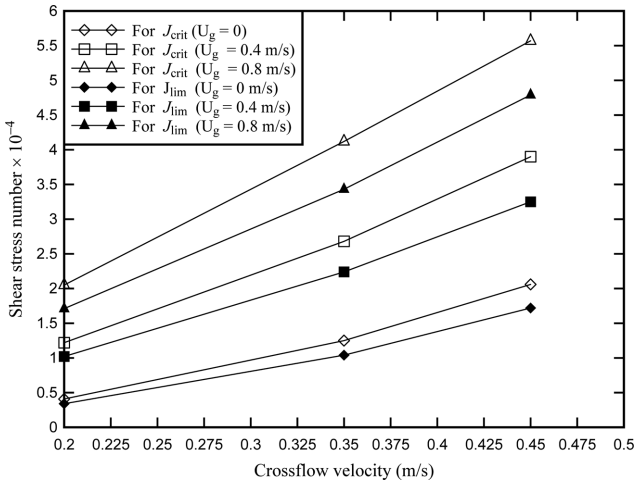

Fig. 5. Shear stress number as a function of cross flow velocity at three different gas sparging conditions (no gas sparging (U_g= 0); gas sparging at U_g=0.4 m/s and gas sparging at U_g=0.8 m/s).

flow velocities (0.2, 0.35 and 0.45 ms^{-1}) were calculated using Eq. (21). Fig. 5 represents shear stress number (N_s) as a function of cross flow velocity during nanofiltration of molasses wastewater at various conditions of gas sparging. The general trend of the plot indicates that with increase in cross flow velocity shear stress numbers increase; however, with gas sparging there is still further enhancement of its magnitude. The shear stress numbers were higher in case of J_{crit} compared to J_{lim} under all experimental conditions. In absence of gas sparging, the shear stress number for J_{crit} at CFV of 0.35 m/s was estimated to be 1.25×10^{-4}, which increased to 2.68×10^{-4} and 4.12×10^{-4} in presence of gas sparging at U_g=0.4 m/s and U_g=0.8 m/s, respectively. The shear stress number for J_{lim} at CFV of 0.45 m/s was estimated to be 1.72×10^{-4}, when there was no gas sparging, but it rose to 3.25×10^{-4} and 4.79×10^{-4} when gas sparging was resumed at gas velocities of 0.4 m/s and 0.8 m/s, respectively. It merits mentioning that the N_s (at the same CFV) for critical flux was much higher than that for limiting flux due to different magnitude of TMP at critical and limiting flux. In absence of gas sparging, N_s increased with the increase in cross-flow velocity. An increase in shear stress number should help reduce concentration polarization and increase the rate of solute removal on the membrane surface, leading to an improvement of permeate flux. A similar trend was reported by other studies [28,31], although in cases of ultra- and microfiltration operations.

4. Permeate Flux

Experiments were conducted to study the effect of gas sparging on the permeate flux behavior in the nanofiltration of molasses wastewater. Fig. 6 represents permeate flux as a function of time for the cases with and without gas sparging (U_g=0 ms^{-1}) at two different constant cross flow velocities of 0.35 and 0.45 ms^{-1}. TMP was maintained at 686 kPa and the concentration of feed solution was 4 kg m^{-3}. Fig. 6 reveals that in absence of any gas sparging there is a gradual drop of permeate flux during 60 min of operation. The flux reduction after 60 min of operation was 19.2% and 26% of the initial flux for cross flow velocities of 0.35 ms^{-1} and 0.35 ms^{-1}, respectively. The magnitude of flux was low, and that of flux reduction was significantly high in case of feed having high initial molasses concentration (data not shown). The trend of flux reduction is presumably due to concentration polarization effect, which is inevitable in any unassisted nanofiltration process. However, the trend reversed as the gas sparging was initiated with two different gas velocities, leading to the gradual recovery of reduced permeates flux.

As Fig. 6 shows, gas sparging resulted in the marked alleviation of flux decline over the entire period of operation. The results indicate that for U_g=0.4 and 0.8 ms^{-1}, although no significant flux enhancement could be observed, there was almost no decline of the permeate flux during the entire 60 min of operation. Thus, it can be inferred that in presence of gas sparging the permeate flux could be maintained over a wide range of experimental conditions. The mitigation of flux decline with gas sparging could be explained by both the shear related enhancement effect (as reflected by shear stress number in Fig. 5) and the presence of secondary flow. When gas is injected into a stationary liquid, such as the situation in submerged membrane systems, bubbles are formed and move upward driven by buoyancy. The bubble motion also generates a secondary flow behind the bubble, i.e., the wake region. Bubble-induced secondary flow plays an important role by promoting local mixing in the bubble wake to minimize the accumulation of the solutes and molecules on the membrane surface [30].

Fig. 7 represents the comparisons of the experimental and theoretical permeate flux values as a function of cross flow velocity for both the cases, in presence and absence of gas sparging, respectively. The general trend of the plot indicates that the permeate flux increases with increase in cross-flow velocity. Also, there was a deviation of 15-20% between the experimental and theoretical flux values. Although data have not been shown, interestingly, most of the deviations occur in the lower feed concentration range. For these experiments, the inaccuracies involved in the flux measurements cannot

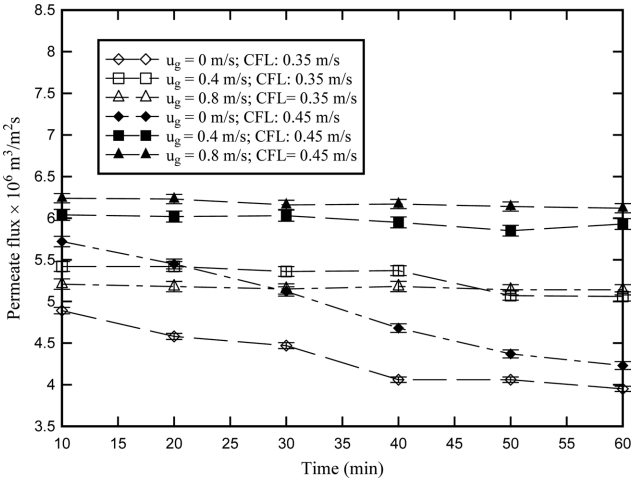

Fig. 6. Time profile of permeate flux with and without gas sparging at two different cross flow velocities (TMP: 686 kPa; concentration of feed soln: 4 kg/m^3; cross flow velocity CFL= 0.35 and 0.45 m/s). (u_g=0 no gas sparging; u_g=0.4 ms^{-1} gas velocity and u_g=0.8 ms^{-1} gas velocity).

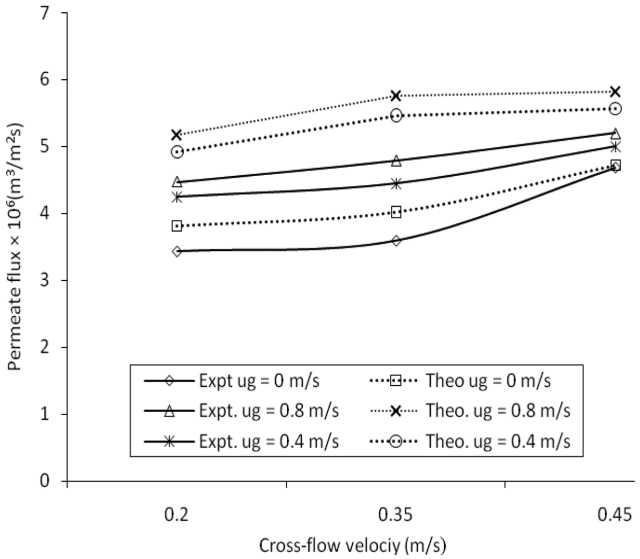

Fig. 7. Experimental and theoretical permeate flux with and without gas sparging with respect to different cross flow velocities (TMP: 686 kPa; concentration of feed soln: 4 kg/m^3). (u_g=0 no gas sparging; u_g=0.4 ms^{-1} gas velocity and u_g=0.8 ms^{-1} gas velocity).

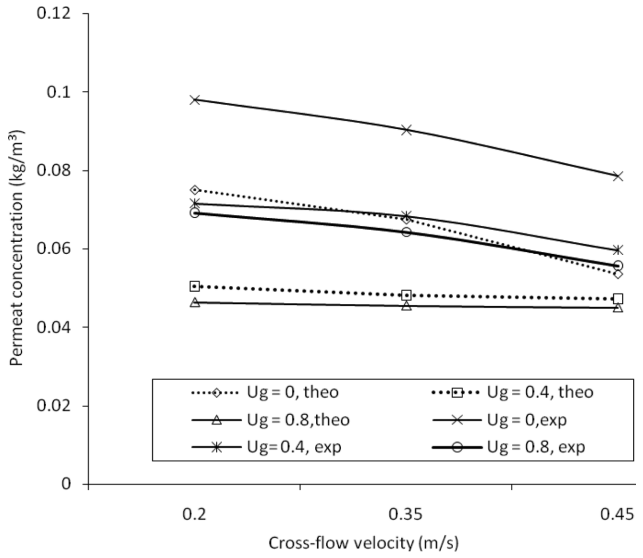

Fig. 8. Experimental and theoretical permeate concentration as a function of crossflow velocity at different gas sparged conditions (TMP: 686 kPa; concentration of feed soln: 4 kg/m^3). (u_g=0 no gas sparging; u_g=0.4 ms^{-1} gas velocity and u_g=0.8 ms^{-1} gas velocity).

be ruled out as a result of fluctuations. This trend of flux increase with increasing cross-flow velocity is quite obvious because higher feed concentration and lower cross flow velocity favor high polarization in absence of gas sparging. Interestingly, there is a drastic reduction of the concentration polarization type layer resistance with gas sparging at higher gas velocities, as discussed earlier.

5. Permeate Concentration

Experimental and theoretical permeate concentration as a function of cross-flow velocity is presented is Fig. 8 for different gas sparging conditions. Permeate concentration decreases with cross flow velocity for all the conditions. Increase in cross flow velocity results in an increase in the forced convection of the solutes, thereby enhancing the solute transport from the membrane surface to the bulk feed. This reduces the concentration of solutes in the permeate stream [31] with increase in cross-flow velocity. The membrane surface concentration decreases due to the sweeping action of the cross flow, so as a result, the permeate concentration decreases [32]. On the other hand permeate concentration increased with increasing TMPs irrespective of cross flow velocities (data not shown), clearly indicating decrease in molasses rejection with increasing pressure. This observation can be explained by the fact that an increase in trans-membrane pressure leads to an increase in both solvent and solute flux. Since solute rejection is a function of both fluxes, a maximal rejection would be reached at a certain transmembrane pressure and solvent flux. This maximal value is dependent on the cross flow velocity. However, the maximum value could not be reached at high TMP and high cross flow velocities [33]. At higher pressure the permeate concentration was more, due to an enhanced con-

Table 2. Effluent discharge and treated spentwash prescribed by the Central Pollution Control Board, India (CPCB)

Parameter	CPCB discharge standards	
	Into surface water, Indian Standards: 2490 (1974)	On land for irrigation, Indian Standards: 3307 (1974)
Temperature (°C)	Shall not exceed 40 °C	Shall not exceed 40 °C
pH	5.5-9.0	5.5-9.0
COD (mg/L)	250	--
BOD_5[a] (at 20 °C) (mg/L)	30	100[b]
Total dissolved solids (mg/L)	200	250

[a]BOD5 was not reported in the present paper

[b]When land is used for secondary treatment, BOD up to 500 mg/L is permissible

Table 3. Qualitative properties of the permeate stream under two different conditions of 'no gas sparging' and 'gas sparging at U_g=0.4 m/s' (CFV: 0.35 m/s)

	No gas sparging					Gas sparging at U_g=0.4 m/s			
Feed composition (mg/L)	ΔP (kPa)	Colour removal (%)	TDS removal (%)	COD kg/m^3	Conductivity (μs/cm)	Color removal (%)	TDS removal (%)	COD kg/m^3	Conductivity (μS/cm)
1000 TDS: 1036 kg/m^3	490	98.58	68.83	116	192.30	98.83	60.1	100	184.61
Conductivity: 1593.8 μs/cm	686	98.64	63.82	107	230.77	98.84	65.10	103	153.84
COD: 2106 kg/m^3	980	98.24	68.27	95	261.54	98.87	60.92	69	384.61
2000 TDS: 1360 kg/m^3	490	98.75	68.44	103	230.77	98.76	67.93	120	292.30
Conductivity: 2092.3 μs/cm	686	98.45	69.78	112	289.23	98.78	68.32	103	230.76
COD: 2018 kg/m^3	980	98.56	65.02	125	369.23	98.75	70.99	120	307.69
4000 TDS: 1345 kg/m^3	490	98.69	77.86	103	235.38	98.81	66.62	132	492.30
Conductivity: 2461.5 μs/cm	686	98.87	80.63	108	400	98.83	71.2	100	476.92
COD: 2179 kg/m^3	980	98.73	68.57	119	476.92	98.63	71.90	62	369.23

vective flux through the membrane because of the higher driving force [34].

6. Permeate Quality

Untreated molasses waste water poses an aesthetic problem due to its color and odor. Consequently, extensive treatment is required before the treated wastewater can meet the stipulated environmental norms (Table 2). Further, a maximum of 15 m^3 of effluent can be generated per kilolitre of alcohol produced as per the Water (Prevention and Control of Pollution) Cess Rule, 1978 specified by the Government of India [35]. Permeate quality was assessed after evaluation of rejection data for the parameters of color, TDS and COD in terms of pollution indices. These data were compared with effluent discharge standards in distilleries, maltries and breweries as given in Table 2. Qualitative properties of the permeate stream are presented in Table 3 for the two cases, with no gas sparging and with gas sparging at U_g=0.4 ms^{-1}. The values of these parameters are mostly within permissible limits of reuse criteria of molasses waste water irrespective of the experimental conditions. As observed from Table 3, the color removal efficiency of the membrane was remarkably high, being in the range of 98.4-98.7%. The visual observation of the permeate samples indicated that they were virtually colorless. It can be conclusively said from this result that the PA-NF membrane with MWCO 250 is good enough to remove the coloring matters, most of which are of larger organics (being polymerized compounds like, caramel). The percent removal of COD was much higher than that of TDS and was in the range of 93-95% compared to that of 65-77% for TDS as shown in Table 3 for either conditions of gas sparging or no sparging. The NF membranes have the unique property of being able to separate both organic and inorganic solutes. Organic compounds being non-ionic in nature compared to the inorganic compounds showed much higher rejection. Further, inorganic solutes are of much smaller molecular mass compared to that of organic compounds, which causes more amounts of inorganic compounds to slip through the membrane compared to that of organic compounds, resulting in higher rejection of organic matters compared to that of inorganic solutes. The nanofiltration membrane with larger pore structures allowed smaller inorganics such as NaCl while retaining most of the larger organic molecules (molasses), thereby contributing to the lesser reduction of TDS. The results also conform to the general mechanism of separation expected from nanofiltration operation and indicate that gas sparging does not have any direct influence on the quality of permeate stream.

7. AFM and SEM Analysis

Atomic force microscopy (AFM) provides a considerable experimental insight into the surface morphology of polymeric membranes. Representative orthographic plots of tapping mode AFM micrographs of the pristine and used PA-NF membranes are presented in Fig. 9. Some details regarding the shape of individual asperities are lost in the AFM images, but the general morphological trend is preserved. The membrane surfaces are not smooth and nodule aggregates are observed. The nodules are seen as the bright high

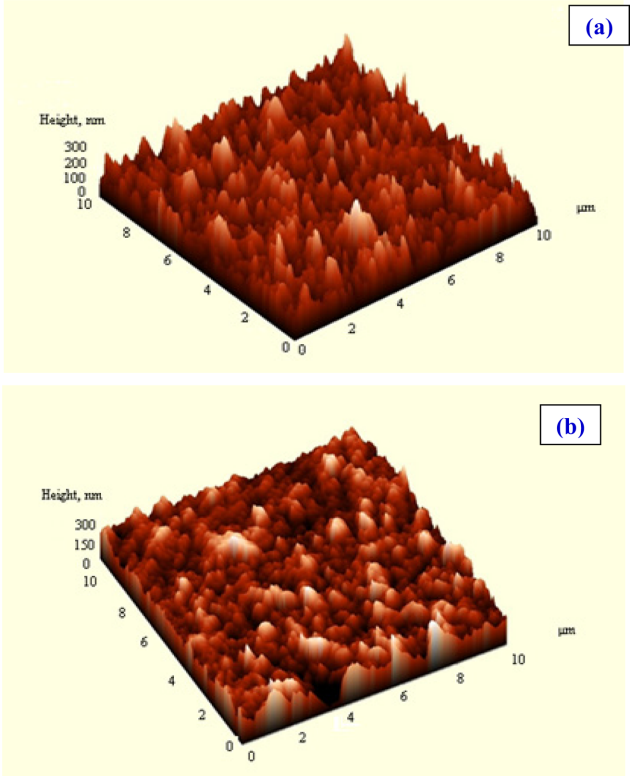

Fig. 9. AFM images of PA-NF membrane (a) unused (b) used membrane.

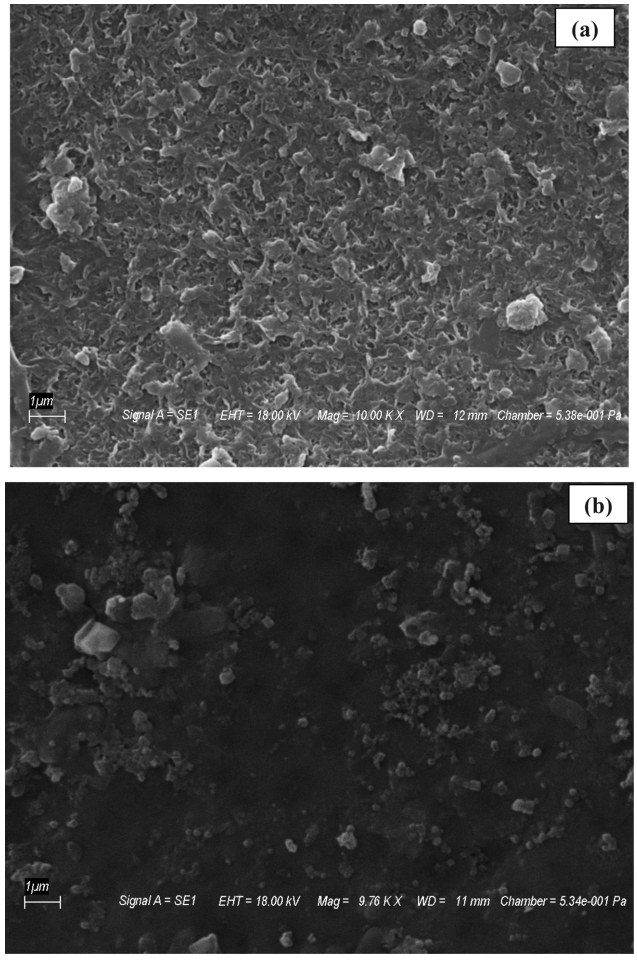

Fig. 10. SEM micrographs of PA-NF membrane (a) unused (b) used membrane.

peaks, whereas the pores are seen as the dark depressions. Fig. 9 indicates that the unused thin-film composite PA-NF membrane exhibits surface roughness of ridge-and-valley structure. The root mean square roughness of the PA-NF membrane was determined to be 0.89 μm. For the used membrane the peaks are still visible, although these are not distinct, as many of them might have shrouded with the solute depositions. For a rough membrane like PA-NF, the particles are preferentially transported into the valleys. The valleys quickly become clogged with the multiple layers of densely packed particles, increasing the cumulative resistance to flow in the valleys and leading to a more rapid loss of flux than for a smooth membrane. The primary influence of the roughness is to reduce the repulsive energy barrier height, thus rendering rough surfaces more favorable for the particle deposition [36].

Fig. 10 shows the SEM micrographs of the PA-NF membrane before (a) and after nanofiltration (b). Both the images were recorded at the accelerating voltage of 18 kV and with the photo angle 45° from normal and the maximum scale bar was 1 μm. The SEM micrograph of the used membrane (Fig. 10(b)) was taken after the completion of the experimental run conducted at maximum TMP of 980 kPa in presence of gas sparging at a velocity of 0.8 m/s for 60 min. Scattered pores are visible on the surface of the pristine membrane and the surface shows flake-like structure. It contains a network of ridges and valleys, which could conceivably trap the organic molecules and inorganic salts, such as those believed to cause fouling on the membrane surface. The SEM images of used membranes were markedly different from those of the new membranes. The micrograph of the used membranes showed a cake of colloidal particles similar to fine sand or silt. This fouling layer completely occluded the active surface of the membrane.

CONCLUSIONS

A semi-empirical resistance-in-series model has been proposed to predict the permeate flux and resistances during the cross flow nanofiltration of molasses wastewater under both the conditions: in presence and absence of gas sparging. Membrane hydraulic resistance, osmotic pressure resistance and the concentration polarization resistance were considered in series. The concentration polarization resistance was correlated to the operating conditions, namely, the feed concentration, the trans-membrane pressure difference and the cross flow velocity for a set of selected experiments. There was an appreciable reduction of concentration polarization resistance R_{cpspar} in presence of gas sparging. Both the concentration polarization resistance R_{cplam} and osmotic pressure resistance R_{osm} decreased with cross-flow velocity, increased with feed concentration and the operating pressure. At a constant feed concentration and trans-membrane pressure the decrease in the membrane surface concentration with cross flow velocity was more pronounced in presence of gas sparging. Experimental and theoretical permeate flux values as a function of cross flow velocity for both the cases, in presence and absence of gas sparging, were compared. The permeate flux increased with increase in cross-flow velocity. There was a deviation of 15-20% between the experimental and theoretical flux values. Although the permeate flux in the nanofiltration could be maintained by the gas sparging, there was no significant change of rejection behavior for the solutes. Similarly, COD and TDS of the permeate streams were also in the same range for both the cases, in absence and presence of gas sparging, but the values were well within the environmental limits. The study of gas-sparged nanofiltration of molasses wastewater confirms that gas sparging is capable of substantial alleviation of flux decline, which is essential for favorable process economics.

ACKNOWLEDGEMENTS

The authors are thankful to Mr. Kishore Bajaj, Technodesign, VU Nagar Gujarat and the Sophisticated Instrumentation Centre for Applied Research and Testing (SICART), Vallabh Vidyanagar, Gujarat, for their valuable help in conducting certain analysis.

NOMENCLATURE

a : osmotic coefficient
c : solute concentration [mg/L] or [kg/m^3]
c_m : membrane surface concentration [mg/L] [kg/m^3]
c_o : feed concentration [mg/L] [kg/m^3]
c_p : permeate concentration [mg/L] [kg/m^3]
C_p : specific heat of solvent
D : diffusivity [m^2/s]
d_e : equivalent diameter [m]
J : permeate flux [m^3/m^{2}s]
J_{crit} : critical flux
J_{lim} : limiting flux
J_w : water flux [m^3/m^{2}s]
k : mass transfer coefficient [m/s]
L : effective membrane length [m]
L_m : thickness of membrane skin [m]
L_p : membrane permeability [m^3/m^{2}s Pa]
M : total mass of the medium in ultrasonic bath
m_1, m_2, m_3 : exponents in Eq. (19)
M_w : molecular weight of solute
n_1, n_2, n_3 : exponents in Eq. (18)
N_s : shear stress number
R : universal gas constant [J/K mole]
R_{ad} : adsorption resistance [m^{-1}]
R_{cp} : concentration polarization resistance
R_{cp}^{spar} : concentration polarization resistance during sparging conditions [m^{-1}]
R_{cp}^{lam} : concentration polarization resistance in laminar flow conditions [m^{-1}]
R_e : Reynolds number, $u_o d_e \rho/\mu$ (dimensionless)
R_m : intrinsic membrane resistance [m^{-1}]
R_{osm} : osmotic pressure resistance [m^{-1}]
R_p : pore blocking resistance [m^{-1}]
R_r : real retention
R_{tot} : summation of a number of resistances
Sc : Schmidt number, μ/ρ D (dimensionless)
Sh : Sherwood number, kd_e/D (dimensionless)
T : temperature [K]
U_g : gas velocity [ms^{-1}]
U_l : cross-flow velocity of liquid [ms^{-1}]
v_w^{osm} : osmotic pressure controlled flux [m^3/m^{2}s]
α : coefficient in Eq. (18)
β : coefficient in Eq. (19)

ΔP : applied pressure difference [Pa]
$\Delta \pi$: osmotic pressure difference across the membrane [Pa]
πm : osmotic pressure at the membrane surface [Pa]
πp : osmotic pressure at the permeate stream [Pa]
μ : feed viscosity [Nm/s]
φ : association factor for solvent
ρ : density of the fluid [kg/m^3]

REFERENCES

1. M. Mayer, R. Braun and W. Fuchs, *J. Membr. Sci*., **277**, 258 (2006).
2. T. Imasaka, N. Kanekuni, H. So and S. Yoshini, *J. Ferment. Bioeng*., **68**, 200 (1989). AWWA, Membrane Technology Research Committee, *J. Am. Water Works Asso.*, **97**, 79 (2005).
3. Z. F. Cui and K. I. T. Wright, *J. Membr. Sci.*, **90**, 183 (1994).
4. S. R. Bellara, Z. F. Cui and D. S. Pepper, *J. Membr. Sci.*, **121**, 175 (1996).
5. S. Chang and A. G. Fane, *J. Membr. Sci.*, **184**, 221 (2001).
6. W. Youravong, Z. Li and A. Laorko, *J. Food Eng.*, **96**, 427 (2010).
7. T.-W. Cheng and L.-N. Li, *Separ. Purif. Technol.*, **55**, 50 (2007).
8. M.-J. Um, S.-H. Yoon, C.-H. Lee, K.-Y. Chung and J.-J. Kim, *Water Res.*, **35**, 4095 (2001).
9. S. Laborie, C. Cabassud, L. Durand-Bourlier and J. M. Laine, *Chem. Eng. Sci*., **54**, 5723 (1999).
10. Z. F. Cui, S. Chang and A. G. Fane, *J. Membr. Sci.*, **221**, 1 (2003).
11. S. Mahimairaja and N. S. Bolan, *In: Third Australian and New Zealand Soil Science Societies Joint Conference 2004*, Sydney, Australia, 5-9 December (2004).
12. A. Drews, H. Prieske, E.-L. Meyer, G. Senger and M. Kraume, *Desalination*, **250**, 1083 (2010).
13. T. Taha and Z. F. Cui, *J. Membr. Sci.*, **210**, 13 (2002).
14. B. G. Fulton, J. Redwood, M. Tourais and P. R. Berube, *Desalination*, **281**, 128 (2011).
15. C. C. V. Chan, P. R. Berube and E. R. Hall, *J. Membr. Sci.*, **297**, 104 (2007).
16. F. FitzGibbon, D. Singh, G. McMullan and R. Marchant, *Proc. Biochem.*, **33**, 799 (1998).
17. S. K. Nataraj, K. M. Hosamani and T. M. Aminabhavi, *Water Res.*, **40**, 2349 (2006).
18. U. K. Rai, M. Muthukrishnan and B. K. Guha, *Desalination*, **230**, 70 (2008).
19. X.-L. Wang, C. Zhang and P. Ouyang, *J. Membr. Sci.*, **204**, 271 (2002).
20. D. E. Wiley, C. J. D. Fell and A. G. Fane, *Desalination*, **52**, 249 (1985).
21. S. De and P. K. Bhattacharya, *J. Membr. Sci.*, **128**, 119 (1997).
22. V. S. Minnikanti, S. DasGupta and S. De, *J. Membr. Sci.*, **157**, 227 (1999).
23. G. B. van der Berg, I. G. Racz and C. A. Smolders, *J. Membr. Sci.*, **47**, 25 (1989).
24. R. E. Treybal, *Mass transfer operations*, 3rd Ed., McGraw Hill, New Delhi, 34 (1981).
25. K. Auddy, S. De and S. DasGupta, *Sep. Purif. Technol.*, **43**, 85 (2005).
26. T. Y. Chiu and A. E. Jame, *J. Membr. Sci.*, **281**, 274 (2006).
27. APHA, American Public Health Association, (2005). *Standard methods for the examination of water and waste-water*, In: Clesceri LS, Greenberg AE, Eaton AD, Editors, Washington, D.C.ISBN 0-8755-3047-8.
28. G. Ducom and C. Cabassud, *Desalination*, **156**, 267 (2003).
29. Q. Y. Li, R. Ghosh, S. R. Bellara, Z. F. Cui and D. S. Pepper, *Sep. Purif. Technol.*, **14**, 79 (1998).
30. A. Laorko, Z. Li, S. Tongchitpakdee and W. Youravong, *Sep. Purif. Technol.*, **80**, 445 (2011).
31. K. Auddy, S. De and S. DasGupta, *Sep. Purif. Technol.*, **40**, 31 (2004).
32. P. Banerjee, S. Dasgupta and S. De, *J. Hazard. Mater.*, **140**, 95 (2007).
33. I. Koyuncu, D. Topacik and M. R. Wiesner, *Water Res.*, **38**, 432 (2003).
34. N. K. Saha, M. Balakrishnan and V. S. Batra, *Resour. Conserv. Recycl*., **43**, 163 (2005).
35. CPCB (Central Pollution Control Board), *Pollution control acts, rules, notifications issued thereunder*, Vol. I. New Delhi: Central Pollution Control Board, Ministry of Environment and Forests, p. 311-2, 501 (1998).
36. E. M. V. Hoek, S. Bhattacharjee and M. Elimelech, *Langmuir*, **19**, 4836 (2003).